Applied Surface Science 399 (2017) 716–720

Contents lists available at ScienceDirect

Applied Surface Science

journal homepage: www.elsevier.com/locate/apsusc

Full Length Article

Transparent conductive Hf-doped In_2O_3 thin films by RF sputtering technique at low temperature annealing

G.H. Wang[a], C.Y. Shi[b,*], L. Zhao[a], H.W. Diao[a], W.J. Wang[a]

[a] Key Laboratory of Solar Thermal Energy and Photovoltaic System of Chinese Academy of Sciences, Institute of Electrical Engineering, The Chinese Academy of Sciences, Beijing 100190, China
[b] China Telecommunication Technology Labs, China Academy of Information and Communication Technology, Beijing 100015, China

ARTICLE INFO

Article history:
Received 23 August 2016
Received in revised form
24 November 2016
Accepted 30 November 2016
Available online 2 December 2016

Keywords:
Transparent conductive oxide films
Hf-doped In_2O_3
Radio frequency sputtering
Hall mobility
Low temperature annealing

ABSTRACT

Hf-doped In_2O_3 transparent conductive polycrystalline films (IHFO) were grown at a low substrate temperature by radio frequency magnetron sputtering for the applications of silicon-based solar cell. The effect of argon flow rate on the electrical and optical properties of the films was investigated. Low temperature thermal treatment improved IHFO films properties, with the optimal Hall mobility of 79.6 cm^2/Vs and resistivity of 3.76×10^{-4} Ω cm. The average transmittance of the 807 nm thick IHFO films in the range of 300–1500 nm was above 83%. The carrier density was utilized to evaluate the plasma wavelength of IHFO conducting film which was 1.8 μm. The optimized IHFO film was then applied to amorphous silicon germanium thin film solar cells as the contacting layer. Compared to the cell without such a layer, the efficiency was higher by 0.35%.

1. Introduction

Transparent conducting oxide films are of considerable interest in many optoelectronic applications such as optical detectors, solar cells and flat-panel displays [1–5]. Employing high mobility (μ) films as electrodes for thin film solar cells is promising for efficiency improvement. Many TCO films with high μ were obtained at either high deposition temperatures or with high-temperature post-thermal treatments, which limited their application to a-Si/c-Si heterojunction (SHJ) or other thin film solar cells fabricated at low temperature [6–9]. Metal-doped In_2O_3 thin film prepared by different method to obtain high mobility has attracted considerable attention. Recently, Meng et al. obtained a maximum μ of 89 cm^2/Vs for In_2O_3:W (IWO) films at lower than 200 °C substrate temperature by reactive plasma deposition (RPD) technique. Consequently, a conversion efficiency of 20.8% was obtained by applying the film to the SHJ solar cell [10]. Kobayashi et al. reported CeO_2-doped hydrogenated In_2O_3 (ICO:H) films deposited by high-density plasma-enhanced evaporation (HPE) with superior μ values of 141 cm^2/Vs. In addition, H-doped In_2O_3 (IO:H) films also showed high μ exceeding 105 cm^2/Vs [11,12]. In most of the aforementioned literature, oxygen was used as a reactive precursor to improve the TCO film properties. However, oxygen usage during deposition complicates the process. So far, there were only very few reports on the μ and transmittance date of Hf-doped In_2O_3 transparent conductive films (IHFO) deposited by magnetron sputtering without oxygen at low substrate temperature.

In this work, the optical, structural and electrical properties of IHFO films were simultaneously investigated for the applications of amorphous silicon germanium (a-SiGe) solar cells, in which it serves as the conductive layer on the rear surface. This study also aims at the reduction of mass production complexity by excluding oxygen as a variable parameter.

2. Experimental details

The IHFO films were deposited on quartz or polished silicon substrates by radio frequency magnetron sputtering from a sintered ceramic HfO_2-doped In_2O_3 (1 wt.%) target in an argon atmosphere. The films were deposited using various argon (Ar) flow rates from 10 to 50 sccm at a substrate of 150 °C. The thickness of the films was measured by a Veeco Dektak 200 surface profiler. The crystalline structures of films were monitored by X-ray diffractometer (XRD) using a Cu-Kα irradiation source. Scanning electron microscopy (SEM) (ZEISS SIGMA) was used to characterize the surface and cross-sectional images. The hafnium (Hf) content in IHFO films was

* Corresponding author.
E-mail address: shichengying@caict.ac.cn (C.Y. Shi).

http://dx.doi.org/10.1016/j.apsusc.2016.11.239
0169-4332/

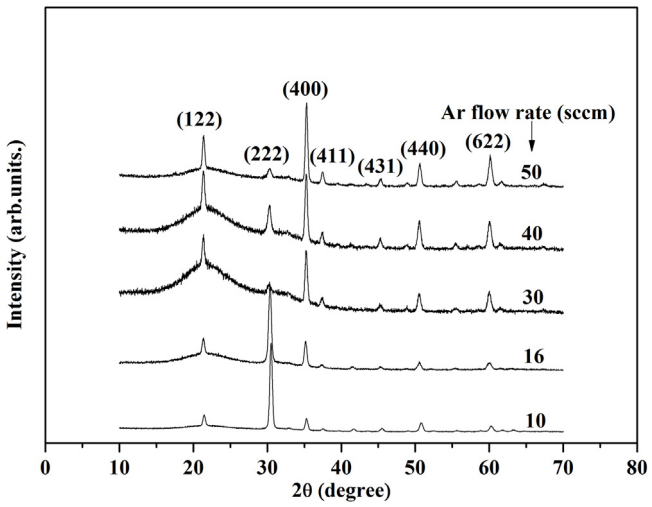

Fig. 1. XRD spectra of IHFO films deposited at different Ar flow rate.

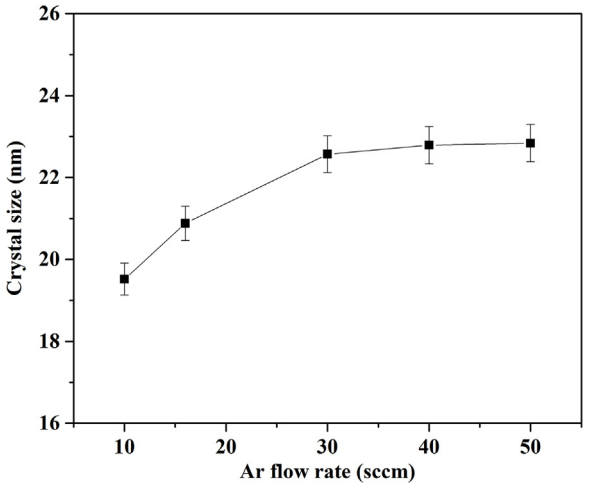

Fig. 2. Crystal sizes of the films calculated using the Scherrer equation from XRD spectra.

analyzed by EDX on the SEM at high voltage of 15.0 kV. The surface morphology and roughness were checked by an atomic force microscopy (AFM) (Bruker Model Icon). The optical reflection and transmittance were measured by a Varian Excalibur HE 3100 UV-Vis-NIR Spectrophotometer. The electrical properties of the IHFO films were analyzed by Hall effect measurement system HL 5500 PC (Nanometrics).

The a-SiGe thin film solar cells were fabricated in a capacitively coupled radio frequency plasma enhanced chemical vapor deposition (RF-PECVD) system with a base vacuum of 10^{-5} Pa. The reactive gases for the deposition were silane (SiH_4), Germane (GeH_4), hydrogen (H_2), diborane (B_2H_6) and phosphine (PH_3). The pressure and flow rates were independently varied by a downstream throttle valve controller and upstream mass flow controllers, respectively. The photo current-density versus voltage (J-V) characteristics of the fabricated solar cells were measured at 25 °C under 1-sun (AM1.5, 100 mW/cm^2) solar simulator radiation.

3. Results and discussion

Fig. 1 shows the XRD patterns of the IHFO films deposited at 10, 16, 30, 40 and 50 sccm Ar flow rates. The thickness of all IHFO films is about 490 ± 30 nm. The films show typical polycrystalline structures with the weak diffraction peaks of (122), (222), (400), (411), (431), (440) and (622) together. The structure is dominated by a strong (222) peak near 30.2° under low Ar flow rates. Its intensity decreases with the Ar flow rate, while other peaks intensify. There is a large increment in the (400) peak intensity at 35°, which corresponds to In_2O_3 with a preferred [100] orientation. It shows that an increment in Ar flow rate favours the preferred orientation along the (400) direction. For ITO films sputtered in pure argon, the preferential orientation along the [100] orientation is always more pronounced at higher RF power [13,14], since higher RF power enhances the mobile energy of sputtered atoms on substrates and hence improves the crystallinity of ITO films. However, for IHFO films deposited at constant RF power, oxygen vacancies concentration might play a role in changing the preferred orientations from (222) to (400) with the Ar flow rate [15–19]. The low concentration of oxygen vacancies leads to more favour to the (111) textured IHFO growth at low Ar flow rate. Moreover, because the high atomic density (111) plane present a lower surface free energy than the (001) plane, the (111) texture should be preferentially observed. When concentration of oxygen vacancies will increase with Ar flow rate, (001) textured IHFO growth is dominant. The growth under high Ar flow rate will lead to In-rich conditions favouring the (001) textured IHFO growth. The incident indium species reach the substrate surface. Such In species will play a key role by acting as an auto surfactant that lowers the surface free energy difference between the (001) and (111) surface [20,21].

The crystal sizes of the films are calculated using the Scherrer Eq. (1) from XRD spectra [22]

$$D_{hkl} = 0.89\frac{\lambda}{\beta\cos\theta} \quad (1)$$

Where D_{hkl} is the crystal size; λ is the X-ray wavelength, β is the FWHM of each peak as a function of 2θ. Furthermore, θ is the Bragg angle. Fig. 2 shows the average crystal sizes of the films calculated using the Scherrer equation from XRD spectra. The crystal size becomes larger with the Ar flow rate, which shows an increment of the film crystallinity. When the crystallinities are low, the grain boundary scattering is dominant. However, thin films are highly crystallized and the ionized impurity scattering is dominant. The ionized impurity scattering might be dominant with the Ar flow rate [23].

Fig. 3 shows the (a) surface and (b) cross-sectional SEM images of an IHFO film on polished Si substrate. The thickness is about 807 nm. The film is deposited uniformly on the Si substrate. A dense granular structure can be observed in the surface scan, while columnar structures perpendicular to the Si substrate is shown in the cross-sectional image. The well crystallized IHFO film agrees with the XRD analysis.

Fig. 4 shows the resistivity (ρ), carrier concentration (n) and μ of the IHFO films as a function of Ar flow rate. It is clear that electrical properties are sensitive to Ar flow rate. The ρ increases from a minimum value of $3.74 \times 10^{-4}\,\Omega$ cm at 16 sccm to $7.84 \times 10^{-4}\,\Omega$ cm, while the μ and n reaches the 50.7 cm^2/Vs and 4.41×10^{20} cm^{-3} respectively at 16 sccm Ar flow rate, and then decreases markedly with the Ar flow rate. The films crystallinity increment does not improve the μ because of smaller grain scattering with the Ar flow rate. IHFO film is an n-type semiconductor. The increment of ionized impurity scattering probably originated from oxygen vacancies might play a role in determining the mobility decrement [24]. The n increases and ρ decreases at low Ar flow rate when the concentration of oxygen vacancies acting as electron donors improves. The concentration of oxygen vacancies will further improve with increasing Ar flow rate, and such vacancies will be close together. This fact might induce the phenomenon of annihilation of oxygen vacancies, which will lead to the creation of neutral In and a decrement in the n, and it follows that the ρ will increase with the Ar flow rate [25].

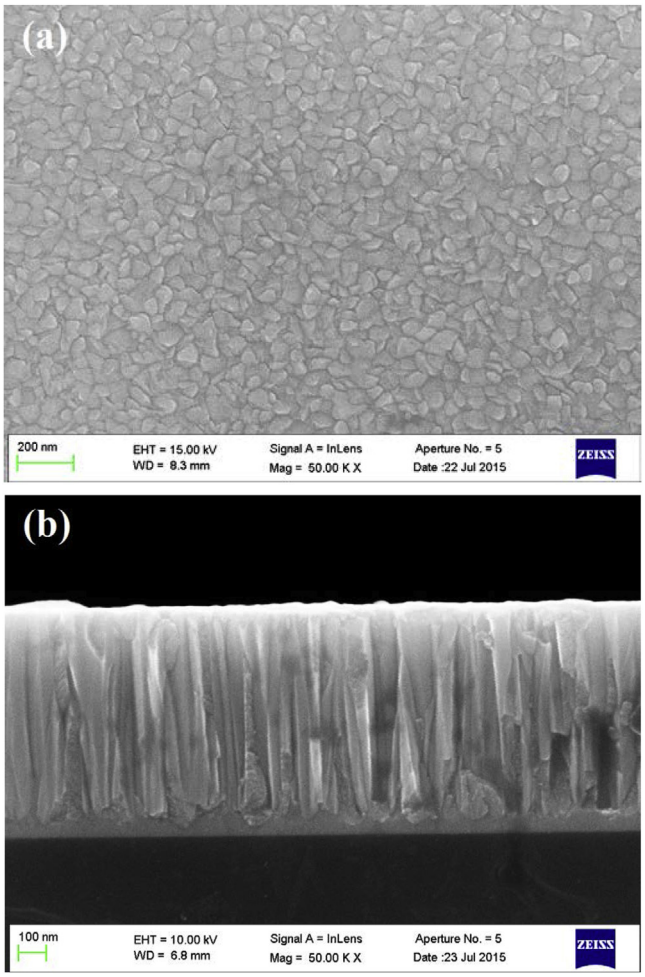

Fig. 3. (a) Surface and (b) cross-sectional SEM images of an 807 nm thick IHFO film uniformly deposited on a polished Si substrate.

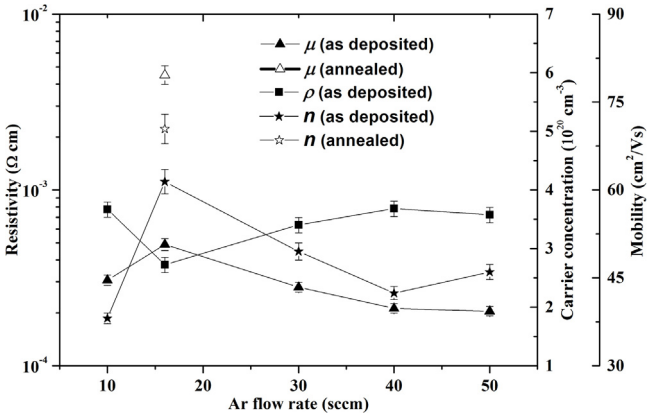

Fig. 4. ρ, n, μ of IHFO films as functions of Ar flow rate and n, μ of IHFO film deposited at 16 sccm Ar flow rate after annealing.

The Hf content in the film by EDX before annealing reaches the 2.82 ± 0.64 Wt.%, which is higher than the one of target. It is deduced that Hf substitutes probably for In site in the indium oxide lattice, furthermore, the incorporation of Hf with O will form the Hf–O complex [10,26].

The annealing plays a dominant role in governing the film growth mechanism which determines the film microstructure and properties. The optimal sample obtained at 16 sccm Ar flow rate is

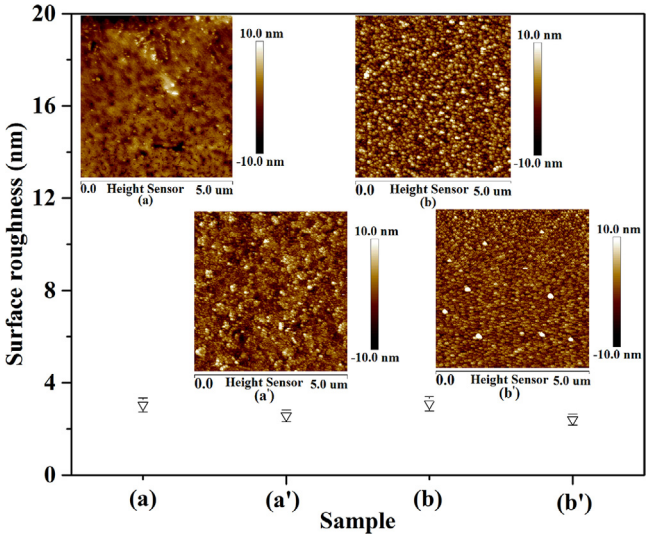

Fig. 5. The surface roughness of different thickness films before ((a) and (b)) and after ((a′) and (b′)) annealing. Film (a) is 436 nm thick and film (b) is 807 nm thick. The insets of figure are surface morphologies of corresponding films before and after annealing.

annealed for 2 h in air at 230 °C. Fig. 4 shows the low temperature annealing process increases μ from 50.7 to 79.6 cm^2/Vs and n from 4.14×10^{20} cm^{-3} to 5.04×10^{20} cm^{-3} at 16 sccm Ar flow rate.

Meng et al. have attributed a higher μ to a higher oxygen partial pressure [10]. In this work, oxygen is not introduced in the sputtering process. Nevertheless, the annealing process in air might reduce the number of oxygen vacancies in the films, which led to a higher μ [27]. Fig. 5 shows the surface roughness of different thickness films before ((a) and (b)) and after ((a′) and (b′)) annealing. The film thickness in (a) and (b) is 436 nm and 807 nm, respectively. The insets of figure are surface morphologies of different thickness films before and after annealing. The root mean square (R_q) of the surface roughness decreases after annealing for both films. The clusters of grain for 436 nm thick film are presented and grains become denser with size increment from 110 ± 10 to 130 ± 10 nm for 807 nm one after the thermal treatment, which leads to less grain boundaries that behave as traps for free carries and barriers for their transport in the films. Hence, less grain boundary scattering leads to a μ improvement.

Many carriers are probably released from the crystallized area. These facts imply that the dopant Hf must be inactive in the amorphous IHFO and become active with raised crystallization during annealing, as reported in some studies [28,29]. So n increases after annealing.

Optical transmittance is considered as one of the most essential properties in evaluating the optical performance of TCO film. Fig. 6 shows the transmittance and reflectance spectra of 807 nm thick IHFO film deposited at 16 sccm Ar flow rate. The inset shows Tauc plot from which the optical band gap (E_g) value of IHFO film is determined. The average transmittance in the range of 300–1500 nm is above 83% and reaches 90% at 550 nm wavelength.

The high μ in TCO film means a larger wavelength transparency limit, which is characterized by the plasma wavelength λ_p. λ_p can be calculated according to the Drude model [10,30–32]

$$\lambda_P = 2\pi c \left(\frac{\varepsilon_0 \varepsilon_\infty m_c^*}{ne^2} \right)^{1/2} \quad (2)$$

Where c is the velocity of light, n is the carrier density, e is the electronic charge, ε_0 is the permittivity of free space, ε_∞ is the high frequency permittivity, $m_c{}^*$ is the conductivity effective mass, ε_∞ and $m_c{}^*$ are assumed as 4 and 0.3 m_e, respectively. λ_p of the IHFO

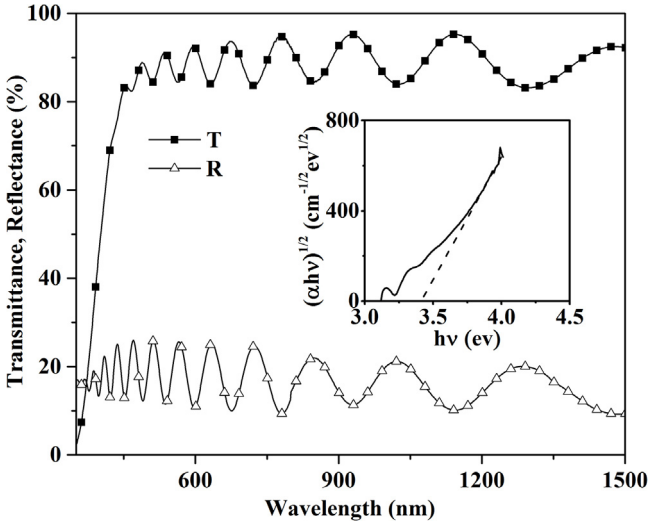

Fig. 6. The transmittance and reflectance spectra of 807 nm thick IHFO film deposited at 16 sccm Ar flow rate. The inset is Tauc plot from which the E_g value of IHFO film is determined.

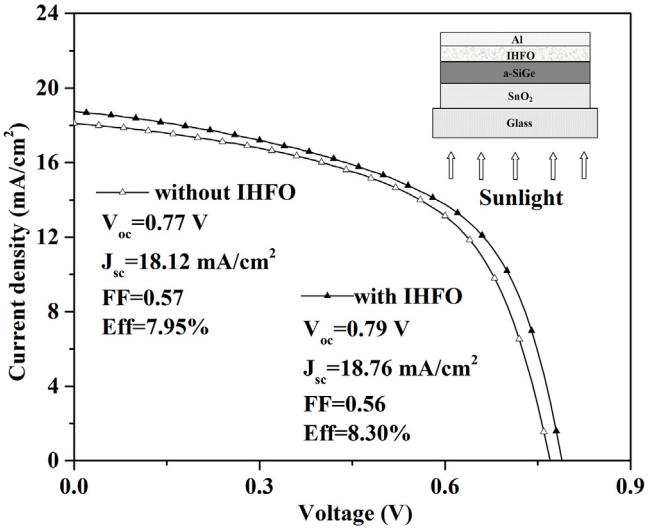

Fig. 7. J-V curves and performance parameters of a-SiGe solar cells with and without IHFO contact layer, the inset of figure is the a-SiGe solar cell schematic diagram in this work.

film deposited at 16 sccm Ar flow rate is then calculated as 1.8 μm. The larger λ_p therefore extends the transparency window into the NIR region.

Based on the transmittance and reflectance data of IHFO films, the E_g calculated is 3.43 eV by Tauc's Eq. (3) [33]

$$(\alpha h\nu)^{1/2} = B\left(h\nu - E_g\right) \tag{3}$$

Where $h\nu$ is the photon energy, B is a constant, α is the absorption coefficient, so that E_g is obtained by extrapolation of the linear fit to $\alpha = 0$.

The absorption coefficient is estimated by the following Formula (4)

$$\alpha = \frac{\ln\left(\frac{(1-R)^2}{T}\right)}{d} \tag{4}$$

Where α is the absorption coefficient, d is the thickness of thin film, R and T is the optical reflection and transmission of thin film, respectively.

The a-SiGe thin film solar cell has been widely investigated for photovoltaic power generation, because of their narrow band gap for use in tandem and triple junction solar cells. At device level, an IHFO film is applied to a-SiGe solar cells as the contact layer. The thickness of the IHFO film is about 80 nm. Fig. 7 shows the performance of the a-SiGe solar cell. The inset of figure is the a-SiGe solar cell schematic diagram in this work. The solar cells are fabricated with the structure of glass/textured SnO_2:F/p-i-n a-SiGe/IHFO/Al. The thickness of a-SiGe layer is 150 nm. It can be observed that, compared to the reference cell without such a contact layer, the efficiency increases by 0.35% by inserting an IHFO layer, mainly due to an increment in the short-circuit current density (J_{sc}). In addition, the open-circuit voltage (V_{oc}) also reaches to 0.79 V.

The external quantum efficiency (EQE) curves of the solar cells with and without IHFO contact layers are shown in Fig. 8. Clearly, EQE of the solar cell with IHFO contact layer dramatically intensifies in the 550–800 nm range compared to the reference. The solar cell performance thus improves to a great extent, in which IHFO film between n-layer and Al back reflector is an effective diffusion barrier to reduce the diffusion of Al atoms into the absorber layer of solar cell [34].

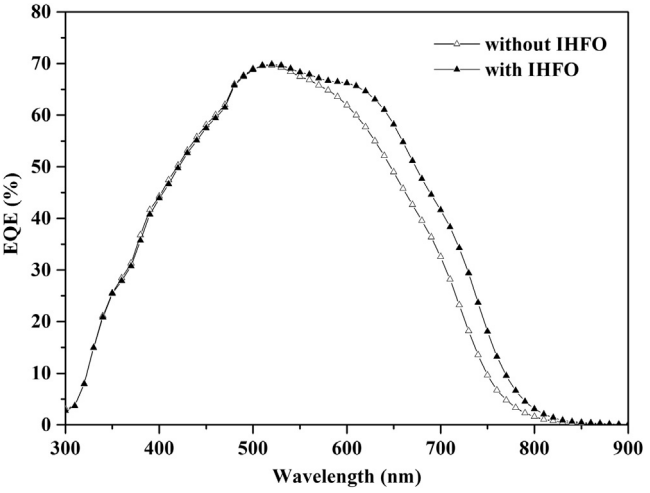

Fig. 8. EQE curves of a-SiGe solar cells with and without IHFO contact layer.

4. Conclusion

In this study, the structural, electrical and optical properties of the IHFO films fabricated by radio frequency magnetron sputtering were investigated. XRD study on the films showed typical polycrystalline structures. The cross-sectional SEM image showed columnar structures perpendicular to the substrate. The film ρ initially reduced from $7.76 \times 10^{-4}\,\Omega\,cm$ to $3.76 \times 10^{-4}\,\Omega\,cm$ at 16 sccm with the Ar flow rate, followed by a sharp increment to $7.84 \times 10^{-4}\,\Omega\,cm$. Low temperature thermal annealing increased the grain size and grain clusters of the IHFO films, resulting in an improved μ and n. Similarly, μ reached to the maximum value of 79.6 cm^2/Vs at the same flow rate. The average transmittance of an 807 nm thick IHFO film in the range of 300–1500 nm was above 83%. Finally, an 80 nm thick film was applied to a-SiGe solar cell as a contact layer. The inclusion of such a layer boosted the EQE in the 550–800 nm range, which translated to an improvement of efficiency of 0.35%. This is mainly attributed to an increment in the J_{sc} of the solar cells.

Acknowledgments

The authors gratefully acknowledge Dr. Jia Ge for revision and discussion. The work is supported by the National Natural Science Foundation of China (61504150) and the China Scholarship Council (201504910179).

References

[1] D.S. Ginley, C. Bright, Transpatent conducting oxides, MRS Bull. 25 (2000) 15–18.
[2] K.L. Chopra, S. Major, D.K. Pandya, Transparent conductors – a status review, Thin Solid Films 102 (1983) 1–46.
[3] Y.J. Lee, H. Park, M. Ju, Y. Kim, J. Park, D.V. Ai, S.Q. Hussain, Y. Lee, S. Ahn, J. Yi, Improvement of haze ratio of DC (direct current)-sputtered ZnO:Al thin films through HF (hydrofluoric acid) vapor texturing, Energy 66 (2014) 20–24.
[4] A. Solieman, M.A. Aegerter, Modeling of optical and electrical proeprties of In_2O_3:Sn coatings made by varous techniques, Thin Solid Films 502 (2006) 205–211.
[5] J.H. Shin, J.S. Lee, C.S. Hwang, S.H. KoPark, W.S. Cheong, M.K. Ryu, C.W. Byun, J.I. Lee, H.Y. Chu, Light effects on the bias stability of transparent ZnO thin film transistors, ETRI J. 31 (2009) 62–64.
[6] D. Zhang, A. Tavakoliyaraki, Y. Wu, R.A.C.M.M. van Swaaij, M. Zeman, Influence of ITO deposition and post annealing on HIT solar cell structures, Energy Procedia 8 (2011) 207–213.
[7] T. Koida, M. Kondo, High-mobility transparent conductive Zr-doped In_2O_3, Appl. Phys. Lett. 89 (2006) 082104-1-3.
[8] R. Hashimoto, Y. Abe, T. Nakada, High mobility titanium-doped In_2O_3, thin films prepared by sputtering/post-annealing technique, Appl. Phy. Exp. 1 (2008) 015002-1-3.
[9] R.K. Gupta, K. Ghosh, S.R. Mishra, P.K. Kahol, High mobility Ti-doped In_2O_3 transparent conductive thin films, Mater. Lett. 62 (2008) 1033–1035.
[10] F.Y. Meng, J.H. Shi, Z.X. Liu, Y.F. Cui, Z.D. Lu, Z.Q. Feng, High mobility transparent conductive W-doped In_2O_3, thin films prepared at low substrate temperature and its application to solar cells, Sol. Energy Mater. Sol. Cells 122 (2014) 70–74.
[11] E. Kobayashi, Y. Watabe, T. Yamamoto, Y. Yamada, Cerium oxide and hydrogen co-doped indium oxide films for high-efficiency silicon heterojunction solar cells, Sol. Energy Mater. Sol. Cells 149 (2016) 75–80.
[12] E. Kobayashi, Y. Watabe, T. Yamamoto, High-mobility transparent conductive thin films of cerium-doped hydrogenated indium oxide, Appl. Phy. Express 8 (2015) 015505-1-4.
[13] S.Q. Hussain, W.-K. Oh, S. Ahn, A.H.T. Le, S. Kim, S.M. Iftiquar, S. Velumani, Y. Lee, J. Yi, Highly transparent RF magnetron-sputtered indium tin oxide films for a-Si:H/c-Si heterojunction solar cells amorphous/crystalline silicon, Mater. Sci. Semicond. Process. 24 (2014) 225–230.
[14] E. Terzini, P. Thilakan, C. Minarini, Properties of ITO thin films deposted by RF magnetron sputtering at elevated substrate temperature, Mater. Sci. Eng.: B 77 (2000) 110–114.
[15] O. Tuna, Y. Selamet, G. Aygun, L. Ozyuzer, High quality ITO thin films grown by dc and RF sputtering without oxygen, J. Phys. D: Appl. Phys. 43 (2010) 055402-1-7.
[16] M. Gulen, G. Yildirim, S. Bal, A. Varilci, I. Belenli, M. Oz, Role of annealing temperature on microstructural and electro-optical properties of ITO films produced by sputtering, J. Mater. Sci.: Mater. Electron. 24 (2) (2013) 467–474.
[17] D. Kim, Y. Han, J.-S. Cho, S.-K. Koh, Low temperature deposition of ITO thin films by ion beam sputtering, Thin Solid Films 377–378 (2000) 81–86.
[18] T.E. Seung-Ik Jun, M.L. McKnight, P.D. Simpson, A. Rack, Statistical parameter study of indium tin oxide thin films deposited by radio-frequency sputtering, Thin Solid Films 476 (2005) 59–64.
[19] S. Venkatachalam, H. Nanjo, F.M.B. Hassan, K. Kawasaki, M. Kanakubo, T. Aizawa, T. Aida, T. Ebina, Characterization of nanocrystalline indium tin oxide thin films prepared by ion beam sputter deposition method, Thin Solid Films 518 (2010) 6891–6896.
[20] M. Nistor, W. Seiler, C. Hebert, E. Mater, J. Perrière, Effects of substrate and ambient gas on epitaxial growth indium oxide thin films, Appl. Surf. Sci. 307 (2014) 455–460.
[21] W. Seiler, M. Nistor, C. Hebert, J. Perrière, Epitaxial undoped indium oxide thin films: structural and physical properties, Sol. Energy Mater. Sol. Cells 116 (2013) 34–42.
[22] B.D. Cullity, Elements of X-Ray Diffraction, Addison-Wesley, New York, 1978.
[23] Ho-Chul Lee, O. Ok Park, Electron scattering mechanisms in indium-tin-oxide thin films: grain boundary and ionized impurity scattering, Vacuum 75 (2004) 275–282.
[24] C. Guillén, J. Herrero, Structure, optical, and electrical properties of indium tin oxide thin films prepared by sputtering at room temperature and annealed in air or nitrogen, J. Appl. Phys. 101 (2007) 073514-1-7.
[25] E. Millon, M. Nistor, C. Hebert, Y. Davila, J. Perrière, Phase separation in nanocomposite indium tin oxide thin films grown at room temperature: on the role of oxygen deficiency, J. Mater. Chem. 22 (2012) 12179–12185.
[26] Z.D. Lu, F.Y. Meng, Y.F. Cui, J.H. Shi, Z.Q. Feng, Z.X. Liu, High quality of IWO films prepared at room temperature by reactive plasma deposition for photovoltaic devices, J. Phys. D: Appl. Phys. 46 (2013) 075103-1-5.
[27] R.K. Gupta, K. Ghosh, S.R. Mishra, P.K. Kahol, High mobility W-doped In_2O_3 thin films: effect of growth temperature and oxygen pressure on structural, electrical and optical properties, Appl. Surf. Sci. 254 (2008) 1661–1665.
[28] H. Morikawa, M. Fujita, Crystallization and decrease in resistivity on heat treatment of amorphous indium tin oxide thin films prepared by d.c. magnetron sputtering, Thin Solid Films 339 (1999) 309–313.
[29] C.H. Yang, S.C. Lee, S.C. Chen, T.C. Lin, The effect of annealing treatment on microstructure and properties of indium tin oxides films, Mater. Sci. Eng. B 129 (2006) 154–160.
[30] I. Hamberg, C.G. Granqvist, Evaporated Sn-doped In_2O_3 films: basic optical properties and applications to energy-efficient windows, J. Appl. Phys. 60 (1986) R123–R159.
[31] T.J. Coutts, D.L. Young, X.N. Li, Characterization of transparent conducting oxides, MRS Bull. 25 (2000) 58–65.
[32] I.A. Rauf, Extraction of free carrier density and mobility from the optical transmission data of tin-doped indium oxide thin films, Mater. Lett. 23 (1995) 73–78.
[33] J. Tauc, A. Menth, States in the gap, J. Non-Cryst. Solids 8–10 (1972) 569–585.
[34] G.H. Wang, L. Zhao, H.W. Diao, W.J. Wang, Optical enhancement by back reflector with ZnO:Al_2O_3 (AZO) of NiCr diffusion barrier for amorphous silicon germanium thin film solar cells, Vaccum 89 (2013) 40–42.